Progress In Electromagnetics Research, Vol. 115, 95–112, 2011

EFFECTS OF ANTENNAS AND PROPAGATION CHANNELS ON SYNCHRONIZATION PERFORMANCE OF A PULSE-BASED ULTRA-WIDEBAND RADIO SYSTEM

Z. Chen and Y. P. Zhang

School of Electrical and Electronic Engineering
Nanyang Technological University, 639798, Singapore

Abstract—Synchronization performance of a pulse-based ultra-wideband (UWB) system is investigated by taking into account of distortions caused by transmitter and receiver antennas and wireless propagation channels in different environments. The synchronization scheme under consideration can be achieved in two steps: a slide correlator and a phase-locked loop (PLL)-like fine tuning loop. Effects of the non-idealities are evaluated by analyzing the distortion of the received UWB pulse and subsequently the synchronization performance of the pulse-based UWB system. It is found that generally a smaller step is required for the sliding correlator due to distortions introduced by the antennas and channels. However, the fine tuning loop can always be stabilized by adjusting the loop parameters. Therefore, synchronization can always be achieved.

1. INTRODUCTION

UWB technology is a promising candidate for low cost, high performance and short range applications [1, 2]. A broad bandwidth of 7.5 GHz, from 3.1 to 10.6 GHz, has been released by the Federal Communications Commission (FCC), allowing a maximum effective isotropic radiated power (EIPR) of -41.3 dBm/MHz [2]. Compared to conventional narrowband (NB) communication system, which occupies a relatively small bandwidth, a UWB radio has to occupy a fractional bandwidth not less than 20% or an absolute bandwidth at least 500 MHz. In impulse-based UWB radios, such a wide bandwidth is realized by transmitting trains of extremely narrow pulses at low

Received 15 January 2011, Accepted 10 March 2011, Scheduled 23 March 2011
Corresponding author: Yue Ping Zhang (eypzhang@ntu.edu.sg).

power spectral density (PSD). Due to the large bandwidth and narrow pulse width, the UWB radio technology offers a variety of competitive features: low probability of interception, high-resolution capability, through-obstacle penetrating property, and robustness over multipath channels. Therefore, UWB technology can be used for high-rate indoor data communications, low-rate data communication, and accurate ranging and localization [3–6].

For a low data rate UWB link, typically a non-coherent receiver is implemented due to the simplicity in hardware architecture, low power consumption, and low energy efficiency [7–9]. However, non-coherent demodulation suffers bandwidth inefficiency and worse sensitivity. Therefore coherent demodulation is needed for high performance communications. A key building function for a coherent receiver is to synchronize the receiver and the transmitter involved. Due to the extremely narrow pulses used in impulse-radio (IR) UWB, great challenges need to be overcome to realize synchronization. A brief overview of synchronization algorithms for DS-UWB is provided in [10]. Matched filter (MF) synchronization based on maximum-likelihood (ML) estimation requires that input series signal be correlated with all possible pulse positions of locally generated template replicas. All correlators operate simultaneously and a large observation pool can be obtained, making the MF synchronization the fastest in acquisition speed and the simplest method in theory. But the complexity and cost in hardware implementation is prohibitive in many practical systems. Instead, a sliding correlator is often used to serially search for the position of received pulse [6]. More closely on the circuit-level implementation, a two-step synchronization method based on a sliding correlator was proposed [11]. Coarse and fine step sizes are used in signal acquisition and tracking stages, respectively. Another synchronization technique based on a sliding correlator uses two sample-and-hold (S/H) circuits to lock to the zero-crossing point of the received pulse [12, 13]. Synchronization is performed in two-steps: search mode detects the crossover point and track mode maintains synchronization using a feedback control loop. Furthermore, a synchronization scheme based on delay-locked loop (DLL) has been developed as well [14, 15]. Finally a synchronization scheme based on phase and frequency synchronizations was discussed in [16, 17]. The phase synchronization is implemented as a sliding correlator to achieve coarse synchronization while the frequency synchronization performs fine tuning. Due to the finite step size of a sliding correlator, synchronization for UWB cannot always be obtained perfectly, leading to a performance loss in demodulation. Therefore, fine tuning is necessary to improve the synchronization. Another concern is the

frequency drifting between transmitter and receiver reference clocks, which necessitate a synchronization scheme with frequency tuning capability.

On the other hand, as signal passes through a transmitting antenna, propagation channel, and a receiving antenna, distortion is introduced [18–20]. Since the synchronization scheme relies on properties of the pulses, effects of antennas and channels should be taken into account. By including the distortions due to antennas and channels, it can be shown that generally more stringent requirements are imposed on the hardware design. However, by adjusting appropriate parameters of the system, the synchronization scheme can always re-lock the receiver to the transmitter in different environments.

This paper is organized as follows. Section 2 presents properties of Gaussian pulses, based on which the synchronization scheme is designed. Impact of Gaussian pulse order on the synchronization scheme will be included as well. In Section 3, a method to calculate the effects of antennas and channels on received pulses is presented, followed which we examine effects of antennas and channels on the synchronization performance. Finally, conclusions are drawn in Section 4.

2. ANALYSIS OF THE SYNCHRONIZATION SCHEME

Different orders of Gaussian pulse have been used in UWB communication systems. Gaussian second (G2) and fifth (G5) derivatives are popular choices [21, 22]. We first analyze Gaussian pulse properties based on G5 pulse, and extend the analysis to other orders of Gaussian pulses in the subsequent parts.

2.1. Basic Properties of Gaussian Pulses

The G5 pulse, as expressed in (1), has the parameters A_{mp} for signal power adjustment and σ^2 as the variance of a Gaussian distribution. By defining the shaping factor as $\alpha = 2\sigma\sqrt{\pi}$ and setting $\alpha = 0.22\,\text{ns}$, the temporal waveform with a unity absolute peak for G5 is given in Figure 1.

$$\text{G5}(t) = A_{mp}\left(-\frac{t^5}{\sqrt{2\pi}\sigma^{11}} + \frac{10t^3}{\sqrt{2\pi}\sigma^9} - \frac{15t}{\sqrt{2\pi}\sigma^7}\right) \times \exp\left(-\frac{t^2}{2\sigma^2}\right) \quad (1)$$

With the above setting of the pulse shaping factor, the pulse spectrum fits perfectly into the FCC radiation mask for UWB, as depicted in Figure 2. The $-10\,\text{dB}$ cutoff frequencies of the pulse are located at 3.24 and 8.67 GHz, leading to a $-10\,\text{dB}$ bandwidth of 5.43 GHz.

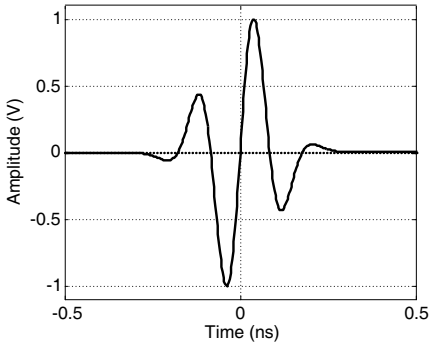

Figure 1. Temporal-domain waveform of a G5 pulse.

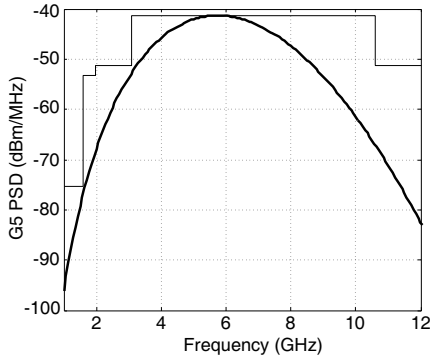

Figure 2. Normalized G5 pulse PSD (thick) and FCC UWB mask (thin).

To receive information from a transmitter using a sliding correlator, correlation properties between the received pulse and the local template play a significant role. For both the local template and the received pulse as G5 pulses, Figure 3 gives the normalized auto-correlation $R_{55}(\tau)$ of the G5 pulse, where the horizontal solid line at 0.4067 indicates the highest sidelobe level $R_{55,\,th}$. During synchronization, the sidelobe level sets a discriminating threshold V_{th} for finding the relative position between the local template and the received pulse. The difference between the mainlobe and the highest sidelobe levels should be as large as possible such that the mainlobe can be easily located against noise and sidelobes for synchronization and demodulation purposes. Due to the symmetry of G5 pulse, $R_{55}(\tau)$ has an even symmetry with respect to the relative delay τ, i.e., when the local template leads or lags the received pulse by the same amount of time, the value of $R_{55}(\tau)$ remains unchanged. To achieve synchronization, the sliding correlator step size $\Delta\tau$ has to be smaller than the effective mainlobe width τ_e, which is defined by mainlobe width intercepted by $R_{55,\,th}$. More specifically, τ_e can be described as

$$R_{55}(\tau) > R_{55,\,th}, \quad \forall\tau \in \tau_e \tag{2}$$

In this particular case, the intercepting points are located ± 30.82 ps, leading to a maximum $\Delta\tau$ as 61.64 ps for the sliding correlator.

With V_{th} and therefore $\Delta\tau$ set by $R_{55,\,th}$, another interesting property between Gaussian fifth and sixth (G6) derivatives can be explored. Unlike the G5 pulse with an odd symmetry, a G6 pulse has an even symmetry. Figure 4 depicts the normalized cross-correlation $R_{56}(\tau)$ between G5 and G6 pulses with respective to the relative delay

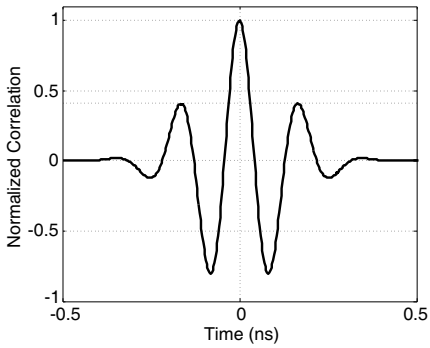

Figure 3. Normalized auto-correlation of R5 pulse (thick) and the highest sidelobe level at 0.4067.

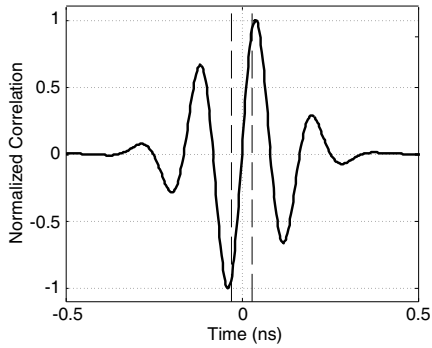

Figure 4. Normalized cross-correlation between G5 and G6 pulses. The two vertical dashed lines indicate the effective main-lobe width of R_{55}.

τ. Instead of the even symmetry for $R_{55}(\tau)$, $R_{56}(\tau)$ has an odd symmetry with respect to τ. More importantly, within the region of τ_e of $R_{55}(\tau)$, i.e., ± 30.82 ps, $R_{56}(\tau)$ monotonically increases. $R_{56}(\tau)$ has a value of zero when G5 and G6 pulses are aligned perfectly, as G5 and G6 pulses are of odd and even symmetries, respectively. A similar monotonic region has been obtained for a Gaussian second derivative in the analysis for an analog impulse radio multiple-access receiver in [23]. In the above analysis, it is assumed particularly that the transmitted signal is a G5 pulse. However, it has been examined that the aforementioned discussions of auto- and cross- correlations are valid for all the orders of Gaussian group pulses [17]. Yet, there are some differences over the change of Gaussian puls order n. With an increase in n, Gaussian pulses have more and higher sidelobes, but narrower mainlobes, resulting in higher sidelobes, narrower mainlobes and therefore lower the value of τ_e in the auto correlations $R_{nn}(\tau)$ and narrower the region of τ_m in the cross correlations $R_{n,\,n+1}(\tau)$. It therefore implies that for a given shaping factor α, a higher order of Gaussian pulse needs a sliding correlator with a smaller step size, imposing more stringent requirements in hardware implementation. For α as 0.22 ns, values of τ_e in $R_{nn}(\tau)$ and τ_m in $R_{n,\,n+1}(\tau)$ are depicted in Figure 5 for Gaussian pulses from the first to the fourteenth derivatives. Unlike for Gaussian pulses with order n greater than 2, for the first and second Gaussian derivatives, τ_m is lower than τ_e. As we will see in the next subsection, the maximum value of $\Delta\tau$ is set by the lower of τ_e and τ_m.

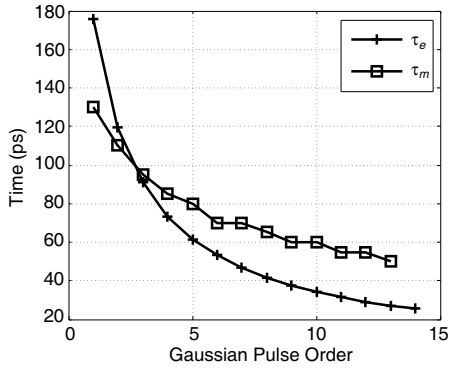

Figure 5. Effective mainlobe width τe and monotonic region width τm over Gaussian pulse orders.

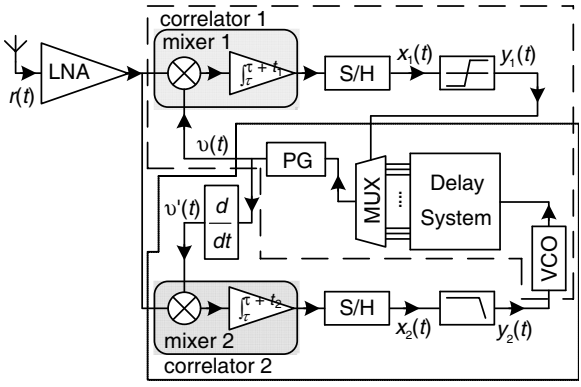

Figure 6. Block diagram for the synchronization scheme in an IR-UWB system.

2.2. Synchronization Scheme

The synchronization scheme based on phase and frequency synchronizations is depicted in Figure 6. As we will analyze, the sliding correlator step size should be limited by the smaller of τ_e and τ_m [17], instead of the pulse width [16]. We will analyze and implement the frequency synchronization in analogy to a PLL as well.

For the ease of analysis of the synchronization mechanism, the signal from a transmitter $s(t)$ is simply expressed as

$$s(t) = \sum_{j=-\infty}^{\infty} A\omega_{tr}(t - jT_f) \tag{3}$$

where A is the signal amplitude, $\omega_{tr}(t)$ is the transmitted pulse waveform, and T_f is the pulse frame time. And the received signal $r(t)$ can be expressed as

$$r(t) = \sum_{j=-\infty}^{\infty} A\omega_{rec}(t - jT_f - \tau_d) \tag{4}$$

where $\omega_{rec}(t)$ is the received pulse waveform and τ_d is to account for the delay. By neglecting the effects of the low-noise amplifier (LNA), the signal at the inputs of mixers 1 and 2 are the same as $r(t)$.

The synchronization can be achieved in two steps, namely phase and frequency synchronizations. The phase synchronization is a pulse-searching process, as shown by the dashed-line box in Figure 6. In order to detect the approximate location of the received pulse $\omega_{rec}(t)$ in the received signal $r(t)$ amplified by LNA, the local template signal $v(t)$, from the pulse generator (PG), is correlated with received signal $r(t)$ first. The template signal $v(t)$ can be expressed as

$$v(t) = \sum_{j=-\infty}^{\infty} \omega_{cor}(t - jT_f - \tau_r) \tag{5}$$

where $\omega_{cor}(t)$ is the energy-normalized template pulse waveform and τ_r the receiver time reference. τ_r is contributed by τ_0, the time reference of the receiver voltage-controlled oscillator (VCO), and τ_j, the delay selected by the multiplexer (MUX) for the jth pulse. The difference $\Delta\tau_{async}$ between τ_d and τ_r is to account for the asynchronism between the transmitter and receiver under investigation. By neglecting effects of antennas and the communication channel in the first-round analysis, the received pulse waveform $\omega_{rec}(t)$ is the same as the template pulse $\omega_{cor}(t)$, which is the G5 pulse.

The output of the correlator 1 for the phase synchronization is then sampled as $x_1(t)$ at a proper time t_1 and compared with the threshold V_{th} which is determined by $R_{55,\,th}$ of the G5 pulse adopted. Finally the decision $y_1(t)$ of the comparator is fed into a multiplexer, which outputs a delayed version of the pulse if no pulse has been detected in the received jth pulse yet. The process keeps going on until V_{th} has been exceeded, i.e., the phase synchronization has been achieved. More specifically, the process can be described by

$$\tau_{j+1} = \begin{cases} \tau_j + \Delta\tau, & \text{if} \quad x_1(t) < V_{th} \\ \tau_j, & \text{if} \quad x_1(t) \geq V_{th} \end{cases} \tag{6}$$

where $\Delta\tau$ is the unit delay of the delay system, i.e., step size of the sliding correlator aforementioned. With N_d defined as the ratio of T_f and $\Delta\tau$, the MUX increases τ_j from zero to $(N_d - 1)\Delta\tau$, and restarts

the process if no pulse has not been detected after one-round search. Therefore, the maximum value of $\Delta\tau$ should be constrained by τ_e of $R_{55}(\tau)$ for the adopted G5 pulse [17], i.e., 61.64 ps.

It can be observed that the phase synchronization by means of the sliding correlator merely finds the approximate location of the received pulse. Taking G5 pulse as an example, phase synchronization may fail to achieve the highest auto-correlation value, given that $\Delta\tau_{async}$ is a random value. More specifically, with the maximum possible output of correlator 1 normalized to unity, phase synchronization is achieved as long as $x_1(t)$ is greater than $R_{55,\,th}$, 0.4067. On the other hand, decision making for the received signal prefers a higher signal-to-noise ratio (SNR), i.e., at a higher correlation value. Therefore, by only phase synchronization, the phase alignment between the transmitter and the receiver involved cannot be achieved completely, which necessitates a fine synchronization. Moreover, to overcome frequency drifting between the transmitter and receiver, frequency tuning is necessary.

Block diagram for the fine synchronization tuning is shown in the dotted box at the bottom of Figure 6. The fine synchronization, namely the frequency synchronization process, only starts to function after phase synchronization has been achieved. $v'(t)$ is obtained by taking derivative on the output of PG once, resulting in a G6 pulse. An S/H block is added as compared with the work in [16]. An intermediate result of the integrator may be misleading and feeds back wrong information to input of the VCO. As a result, output of correlator 2 is only valid at the end of the locally generated pulse, leading to the S/H circuit. The sampled output of correlator 2, $x_2(t)$, is fed into a low-pass filter (LPF) to remove high frequency components, and eventually $y_2(t)$ is passed to the input of VCO. Essentially the fine pulse-position adjustment is performed by varying VCO output frequency. This is equivalent to a PLL. Generally, the transient response of a PLL cannot be analyzed linearly whereas the whole system is typically investigated in the frequency domain [24–26]. Conceptually, together with the S/H block, correlator 2 functions as a phase detector, which activates the VCO in a manner of negative feedback.

To ensure that synchronization is always maintained to the received signal $r(t)$, the frequency tuning loop is designed in an analogy to a 3rd order type II PLL. The PLL is assumed to be implemented with a charge pump and the LPF is expressed as

$$G_{LPF}(s) = \frac{s/\omega_z + 1}{s(s/\omega_p + 1)} \tag{7}$$

where ω_p and ω_z are the pole and zero locations in angular frequency. The second pole at origin is to avoid discrete voltage steps at the VCO control port due to the instantaneous change at the charge

pump output. Therefore the loop transfer function for the frequency synchronization can be expressed as

$$A(s) = K_{PD}\frac{s/\omega_z + 1}{s(s/\omega_p + 1)}\frac{K_{VCO}}{s} = K\frac{s/\omega_z + 1}{s(s/\omega_p + 1)}\frac{1}{s} \tag{8}$$

where K_{PD} and K_{VCO} are the gains of the PD and VCO, respectively. The parameter K is the loop gain as a product of K_{PD} and K_{VCO}. The PLL -3 dB bandwidth is set to one tenth of the input reference frequency, which is the inverse of the frame time T_f. By setting zero frequency ω_z to a fraction of the PLL -3 dB bandwidth, and ensuring a proper phase margin, the frequency synchronization loop can be designed to have the parameters in Table 1. With the design parameters, a phase margin of 61.3 degrees can be obtained for the frequency synchronization loop. As an illustration, the sampled $x_1(t)$ in the phase synchronization loop and LPF output in the frequency synchronization loop are depicted in Figure 7, where the value of $x_1(t)$ at unity indicates perfect synchronization.

3. EFFECTS OF ANTENNAS AND PROPAGATION CHANNELS

Propagation channels and antennas of a UWB link behave as filters on UWB signal. A method to calculate effects of antennas and freespace channel on a received pulse will be introduced first. Distortions on the received pulse will be evaluated for the presented synchronization scheme. Finally, simulations are performed to check the effects of different practical UWB multipath propagation channels on the presented synchronization method.

Table 1. Frequency synchronization parameters for an ideal G5 pulse.

Parameter	Design Value
ω_p	15.3 MHz
ω_z	1 MHz
K_{PD}	2.06 V/s
K	23.9e12 GHz/V
K_{VCO}	1.8455e12 Hz/V

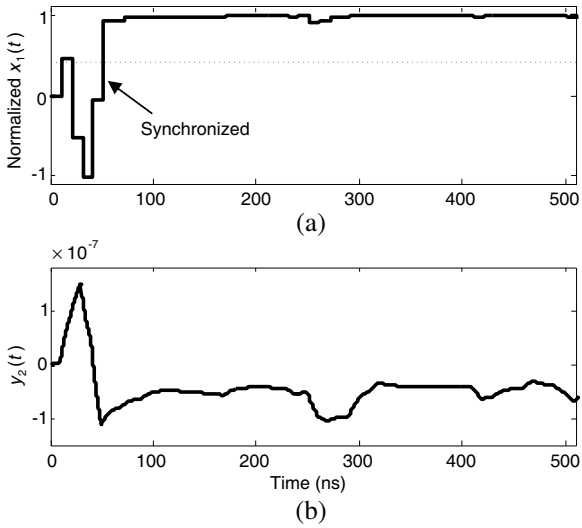

Figure 7. (a) Normalized $x_1(t)$ and (b) LPF output $y_2(t)$ for ideal channel and no antenna. Horizontal dashed line indicates the threshold $R_{55,th}$.

3.1. Calculation of the Received Pulse with Antennas and Freespace Propagation Channel

As the generated pulse is transmitted through a transmitting antenna, a specific propagation channel, and a receiving antenna, distortions are introduced to the received pulse. Therefore, it is important to evaluate the distortion and its effects on the presented synchronization technique.

Planar monopole UWB antennas are popular choices for UWB communications due to their attractive electrical, mechanical and economical merits [27–34]. Normalized transfer functions, $H_{N,Tx}(f)$ and $H_{N,Rx}(f)$, of planar monopole UWB transmitting and receiving antennas [35] can be obtained, respectively [19]. The frequency domain expression, $\omega_{tr}(f)$, of a generated single temporal Gaussian pulse $\omega_{tr}(t)$ is obtained using Fourier transform (FT) and the corresponding received signal frequency-domain expression $\omega_{rec}(f)$ is related to $\omega_{tr}(f)$ by $\omega_{rec}(f) = \omega_{tr}(f)\ S_{21}(f)$. From [19], $S_{21}(f)$ can be expressed as

$$S_{21}(f) = \frac{j\lambda}{4\pi d} H_{N,Tx}(f) H_{N,Rx}(f) \exp\left(-j2\pi f \frac{d}{c}\right) \tag{9}$$

where λ, d, and c are the wavelength, transmitter-receiver distance and light speed in freespace, respectively.

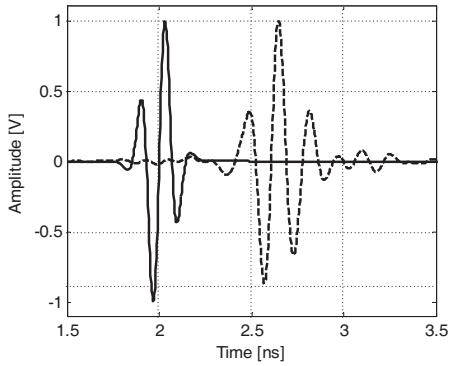

Figure 8. Transmitted (solid line) and received (dashed line) pulses.

The temporal waveform $\omega_{rec}(t)$ at receiver can be obtained using inverse Fourier transform (IFT). Freespace transmission is considered in (9). Taking G5 pulse as the transmitted signal, the transmitted and received temporal pulses with unity peaks are shown in Figure 8. The transmitter-receiver separation is assumed as 20 cm for the ease of observation. Attenuation effect has been removed by normalizing the absolute peak to unity. It can be observed that the distortion, introduced by antennas and the freespace channel, creates stronger sidelobes and alters the temporal waveform somehow between G5 and G6 pulses.

3.2. Impairments of Antennas and the Freespace Propagation Channel on a Received Pulse

Due to distortions in the mainlobe and stronger sidelobes of $\omega_{rec}(t)$, $R'_{55}(\tau)$ has been distorted as well. The highest sidelobe $R'_{55,\,th}$ increases 0.4068 in ideal case to 0.6309 due to distortions in $\omega_{rec}(t)$, leading to smaller effective mainlobe width τ'_e from -22.55 ps to $+21.115$ ps rather than ± 25.33 ps in ideal case. Therefore, the maximum sliding correlator step size $\Delta\tau$ for phase synchronization becomes 43.665 ps, which is smaller as compared with 50.66 ps for an ideal G5 pulse.

Besides $R'_{55}(\tau)$ for the phase synchronization, it is found that the slope S of $R'_{56}(\tau)$, proportional to the gain of the PD, is slightly less than that of $R_{56}(\tau)$ for the ideal case. Therefore one has to take the change of S into account when setting parameters in circuit design. More importantly, $R'_{56}(\tau)$ is located at a positive value, i.e., non-zero, when the involved transmitter and receiver are synchronized. A zero correlation is obtained when the local G6 pulse leads $\omega_{rec}(t)$ by certain

amount of time. In other words, when the output of the correlator 2 is zero, the actual relative position is that the local G6 pulse leads $\omega_{rec}(t)$ by certain amount of time. Therefore, some sort of level shifting in circuit implementation is necessary to restore the correlation to zero at perfect synchronization.

3.3. Effects of Antennas and Multipath Propagation Channels on the Synchronization Scheme

Freespace transmission is assumed in the above-mentioned discussion for effects on received pulses. Multipath is not present due to the ideality of freespace channel. Practical multipath UWB channel can be simulated based on IEEE 802.15.SG3a channel model [36]. By selecting proper values for the arrival rates, decay rates, and standard deviations for different scenarios, a multipath UWB channel can be obtained.

By replacing the term $\exp(-j2\pi fd/c)/d$ in (9) with the channel frequency domain transfer function, the received signal with effects of antennas and the UWB multipath propagation channel can be obtained [18]. For the scenario with line of sight (LOS) and range 0 to 4 meters (case A), the correlation between the received pulse and ideal G5 has the highest normalized sidelobe level $R_{55,\,th}$ at 0.5985, and a phase synchronization step size $\Delta\tau$ as 39.5587 ps, as compared in Table 2. The synchronization can be achieved by changing the

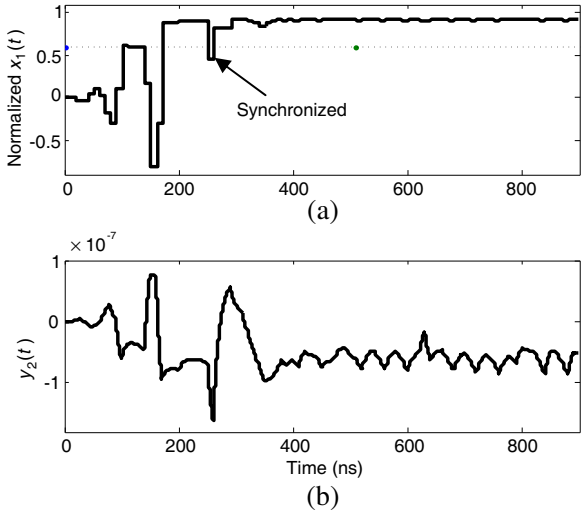

Figure 9. Synchronization performance for IEEE UWB channel Case A. (a) Normalized $x_1(t)$ and threshold at 0.5985; (b) LPF output $y_2(t)$.

sliding correlator step size and VCO gain, and keeping the loop gain loop gain K the same, as shown in Figure 9.

Another application for UWB as lifestyle and medical applications is the wireless connectivity in a body-area network (BAN), which has a shorter coverage than the IEEE 802.15.SG3a channel [37]. Radiographs of path loss and delay spread are provided in [37]. During measurements, the transmitting antenna was placed on the right upper arm and the receiving antenna on testing points of a cylindrical distribution. For a LOS channel measured in a staff lounge, including the effects of UWB antennas, the autocorrelation parameters are included in Table 2. By redesigning the sliding correlator step size and VCO gain, the loop gain K can be kept constant. Thus synchronization still can be achieved, as depicted in Figure 10.

As a viable candidate for short-range high-rate communications, UWB has been applied for intra/inter-chip communications, where

Table 2. Autocorrelation parameters for different UWB channels.

	Freespace	IEEE	BAN	Inter-chip
$R_{55,th}$	0.4067	0.5985	0.6307	0.6142
τ_e (ps)	61.64	39.5587	37.6159	49.5654

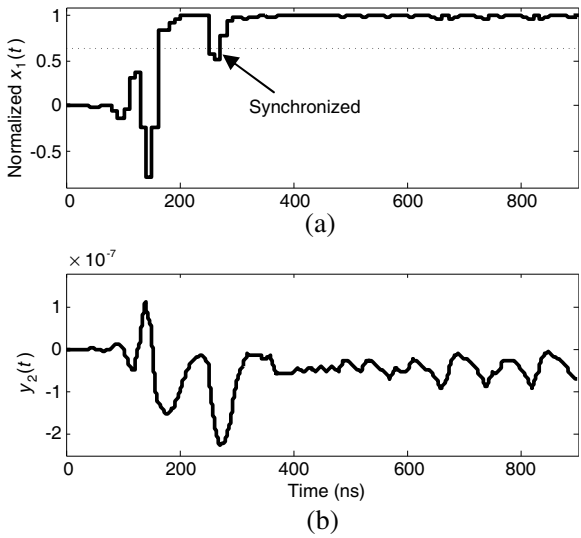

Figure 10. Synchronization performance for UWB BAN channel. (a) Normalized $x_1(t)$ and threshold at 0.6307; (b) LPF output $y_2(t)$.

the transmitter-receiver separation is only up to a few tens of centimeters [4]. Radio propagation channel for inter-chip wireless communications has been modeled based on measurements performed in computer enclosures [38]. To check the performance of the presented synchronization scheme for inter-chip wireless communications, a simulation for non-LOS (NLOS) scenario has been performed as depicted in Figure 11. Compared to the IEEE 802.15.SG3a UWB channel, denser multipaths but a shorter delay spread has been observed due to the contained environment for inter-chip applications. With properly redesigned synchronization parameters, synchronization can be achieved.

From simulations over different multipath propagation channels, including the effect of UWB antennas, it can be concluded that, generally, more stringent requirement is imposed on the hardware design. Due the distortion introduced by the antennas and channels, a smaller step size is required for the sliding correlator. Moreover, the fine synchronization parameters have to be redesigned to accommodate the change of the crosscorrelation properties.

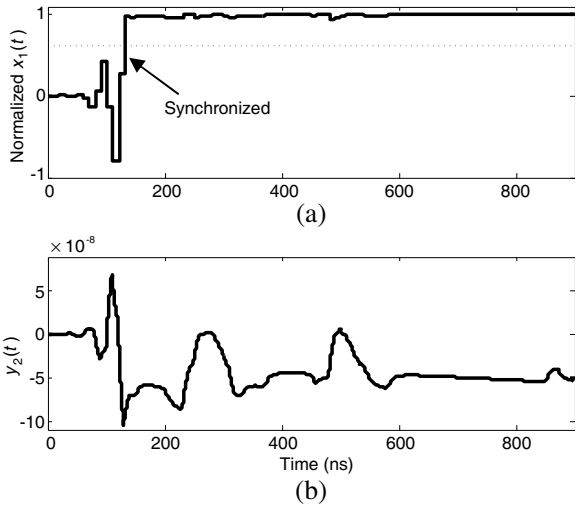

Figure 11. Synchronization performance for UWB inter-chip channel. (a) Normalized $x_1(t)$ and threshold at 0.6142; (b) LPF output $y_2(t)$.

4. CONCLUSION

Synchronization is a critical issue in impulse-based UWB communication systems as extremely narrow pulses are used. With properties on Gaussian group pulses, a synchronization scheme has been presented

and analyzed based on a sliding correlator and a PLL to perform the approximate pulse-searching and the fine pulse-position adjustment respectively. Intuitive explanations for the PLL-based frequency synchronization have been provided. Moreover, differences between a conventional PLL and the PLL-based frequency synchronization have been identified to offer insights for the synchronization scheme design. Tradeoffs in selecting the Gaussian pulse order have been discussed based on ease of circuit implementation and superiority in system performance.

As antennas and propagation channels introduce distortions on the received pulse, a method for evaluating the detrimental effects of the distortions on the presented synchronization scheme has been introduced. With antennas, it has been found that a smaller step size for phase synchronization has to be used as compared to the case without antenna effects. For more realistic scenarios, simulations with different practical UWB multipath channels have been performed. It has been found that a smaller sliding correlator step size is required for the synchronization scheme. Moreover, the frequency synchronization loop parameters have to be redesigned to accommodate the distortions introduced by the antennas and channels. It is a challenging task to design a set of general loop parameters for all the different channels.

ACKNOWLEDGMENT

The authors would like to thank Dr. M. Sun for providing data of the UWB antennas used for discussions.

REFERENCES

1. Win, M. Z. and R. A. Scholtz, "Impulse radio: How it works," *IEEE Commun. Lett.*, Vol. 2, No. 2, 36–38, Feb. 1998.
2. FCC, "In the matter of revision of Part 15 of the commission's rules regarding ultra-wideband transmissions systems," *Federal Commun. Commission First Report and Order*, 02–48, Apr. 2002.
3. Cramer, R. J., R. A. Scholtz, and M. Z. Win, "Evaluation of an ultra-wideband propagation channel," *IEEE Trans. Antennas Propag.*, Vol. 50, No. 5, 561–570, May 2002.
4. Sun, M. and Y. P. Zhang, "Performance of inter-chip RF-interconnect using CPW, capacitive coupler, and UWB transceiver," *IEEE Trans. Microw. Theory Tech.*, Vol. 53, No. 9, 2650–2655, Sep. 2005.
5. Lee, J. L. and R. A. Scholtz, "Ranging in a dense multipath

environment suing an UWB radio link," *IEEE J. Sel. Areas Commun.*, Vol. 20, No. 9, 1677–1683, Dec. 2002.

6. Terada, T., S. Yoshizumi, M. Muqsith, Y. Sanada, and T. Kuroda, "A CMOS ultra-wideband impulse radio transceiver for 1-mb/s data communications and ±2.5-cm range finding," *IEEE J. Solid-State Circuits*, Vol. 41, No. 4, 891–898, Apr. 2006.
7. Lee, F. S. and A. P. Chandrakasan, "A 2.5 nJ/bit 0.65 V pulsed UWB receiver in 90 nm CMOS," *IEEE J. Solid-State Circuits*, Vol. 42, No. 12, 2851–2859, Dec. 2007.
8. Rychaert, J., M. Verhelst, M. Badaroglu, S. D'Amico, V. De Heyn, C. Desset, P. Nuzzo, B. Van Poucke, P. Wambacq, A. Baschirotto, W. Dahaene, and G. Van der Plas, "A CMOS ultra-wideband receiver for low data-rate communication," *IEEE J. Solid-State Circuits*, Vol. 42, No. 11, 2515–2527, Nov. 2007.
9. Chandrakasan, A. P., et al., "Low-power impulse UWB architectures and circuits," *Proceedings of the IEEE*, Vol. 97, No. 2, 332–352, Feb. 2009.
10. Chen, J. and Z. Zhou, "The overview of synchronization in DS-UWB," *Proc. IEEE International Symp. on Communications and Information Technology*, Vol. 2, 983–986, Oct. 2005.
11. Bing, H., X. Hou, X. Yang, T. Yang, and C. Li, "A "two-step" synchronous sliding method of sub-nanosecond pulses for ultra-wideband (UWB) radio," *Proc. IEEE International Conf. on Communications, Circuits and Systems and West Sino Expositions*, Vol. 1, 142–145, Jun. 2002.
12. Deparis, N., C. Loyez, M. Fryziel, A. Boe, N. Rolland, and P. A. Rolland, "Transposition of a base band ultra wide band width impulse radio signal at 60 GHz for high data rates multiple access indoor communication systems," *Proc. IEEE 34th European Microwave Conf.*, Vol. 1, 105–108, Oct. 2004.
13. Deparis, N., A. Boe, C. Loyez, N. Rolland, and P.-A. Rolland, "Receiver and synchronization for UWB impulse radio signals," *Proc. IEEE MTT-S International Microwave Symp. Digest*, 1414–1417, Jun. 2006.
14. Tchikawa, S. and S. Sumi, "A novel delay locked loop for UWB-IR," *Proc. IEEE International Workshop on Ultra Wideband Systems Joint with Conf. on Ultrawideband Systems and Technologies*, 273–277, May 2004.
15. Zhang, W., H. Shen, Z. Bai, and K. S. Kwak, "Design of delay-locked loop (DLL) with low jitter and high lose lock time in UWB-IR system," *Proc. IEEE Asia-Pacific Conf. on Commun.*, 1–5, Aug. 2006.

16. Sasaki, N., P. K. Saha, and T. Kikkawa, "The development of UWB Gaussian monocycle pulse synchronization circuit based on 0.18-µm CMOS technology," [Online]. Available: http://www.rcis.hiroshima-u.ac.jp/21coe/pdf/4th_WS/poster20-p72.pdf.
17. Chen, Z. M. and Y. P. Zhang, "A modified synchronization scheme for impulse-based UWB," *International Conference on Information, Communications, and Signal Processing*, 1–5, Dec. 2007.
18. Sibille, A., "About the role of antennas in UWB impulse radio," *The 9th Management Committee Meeting of COST Action 273, COST273 TD (04)*, Athens, OH, Greece, Jan. 2004.
19. Ma, T. G. and S. K. Jeng, "Planar miniature tapered-slot-fed annular slot antennas for ultrawide-band radios," *IEEE Trans. Antenna Propag.*, Vol. 53, No. 3, 1194–1202, Mar. 2005.
20. Li, Z. Q., C. L. Ruan, and L. Peng, "Design and analysis of palanar antenna with dual WLAN Band-notched for integrated bluetooth and UWB applications," *Journal of Electromagnetic Waves and Applications*, Vol. 24, No. 13, 1817–1828, 2010.
21. Kim, H., D. Park, and Y. Joo, "All-digital low-power CMOS pulse generator for UWB system," *Electron. Lett.*, Vol. 40, No. 24, 1534–1535, Nov. 2004.
22. Xie, H., X. Wang, A. Wang, B. Qin, H. Chen, Y. Zhou, and B. Zhao, "A varying pulse width second order derivative Gaussian pulse generator for UWB transceiver in CMOS," *IEEE ISCAS 2007*, 2794–2797, May 2007.
23. Win, M. Z. and R. A. Scholtz, "Ultra-wide bandwidth time-hopping spread-spectrum impulse radio for wireless multiple access communications," *IEEE Trans. Commun.*, Vol. 48, No. 4, 679–691, Apr. 2000.
24. Gardner, F. M., *Phaselock Techniques*, 3rd edition, Wiley, Jul. 2005.
25. Abramovitch, D., "Phase-locked loops: A control centric tutorial," *Proc. IEEE American Control Conf.*, Vol. 1, 1–15, 2002.
26. Razavi, B., "Design of monolithic phase-locked loop and clock recovery circuits — A tutorial," *Monolithic Phase-locked Loops and Clock Recovery Circuits: Theory and Design*, IEEE Press, Piscataway, NJ, 1996.
27. Chen, Y. and Y. P. Zhang, "Integration of ultra-wideband slot antenna on LTCC substrate," *Electron. Lett.*, Vol. 40, No. 11, 645–646, May 2004.

28. Song, H. W., J. N. Lee, J. K. Park, and H. S. Lee, "Design of ultra wideband monopole antenna using parasitic open loops," *Journal of Electromagnetic Waves and Applications*, Vol. 23, No. 5–6, 561–570, 2009.
29. Faraji, D. and M. N. Azarmanesh, "A novel modified head-shaped monopole antenna for UWB applications," *Journal of Electromagnetic Waves and Applications*, Vol. 23, No. 10, 1291–1301, 2009.
30. Wang, J. J., Y. Z. Yin, and X. W. Dai, "A novel fractal triangular monopole antenna with notched and truncated ground for UWB application," *Journal of Electromagnetic Waves and Applications*, Vol. 23, No. 10, 1313–1321, 2009.
31. Marynowski, W. and J. Mazur, "Design of UWB coplanar antenna with reduced ground plane," *Journal of Electromagnetic Waves and Applications*, Vol. 23, No. 13, 1707–1713, 2009.
32. Abdollahvand, M. and G. R. Dadashzadesh, "Compact double-fed dual annular ring printed monopole antenna for UWB application," *Journal of Electromagnetic Waves and Applications*, Vol. 23, No. 14–15, 1969–1980, 2009.
33. Yang, Y.-B., F.-S. Zhang, L. Zhang, F. Zhang, and Y.-C. Jiao, "Design of a planar monopole antenna with dual band-notched characteristics for ultra-wideband applications," *Journal of Electromagnetic Waves and Applications*, Vol. 23, No. 17–18, 2481–2489, 2009.
34. Zheng, Z.-A., Q.-X. Chu, and T.-G. Huang, "Compact ultra-wideband slot antenna with stepped slots," *Journal of Electromagnetic Waves and Applications*, Vol. 24, No. 8–9, 1069–1078, 2010.
35. Sun, M., Y. P. Zhang, and Y. L. Lu, "Miniaturization of planar monopole antenna for ultrawide-band radios," *IEEE Trans. Antennas Propagat.*, Vol. 58, No. 7, 2420–2425, Jul. 2010.
36. IEEE 802.15.SG3a, "Channel modeling sub-committee report final," *IEEE P802.15-02/460r1-SG3a*, Feb. 2003.
37. Zhang, Y. P. and Q. Li, "Performance of UWB impulse radio with planar monopoles over on-human-body propagation channel for wireless body aread network," *IEEE Trans. Antennas Propagat.*, Vol. 55, No. 10, 2900–2906, Oct. 2007.
38. Chen, Z. M. and Y. P. Zhang, "Inter-chip wireless communication channel: Measurement, characterization, and modeling," *IEEE Trans. Antennas Propagat.*, Vol. 55, 978–986, Mar. 2007.